INTERNATIONAL JOURNAL OF HEALTH & MEDICAL RESEARCH
ISSN(print): 2833-213X, ISSN(online): 2833-2148
Volume 05 Issue 07 July 2026
DOI : 10.58806/ijhmr.2026.v5i7n19
Page No. 720-726

Preparation of Titanium Dioxide Nanoparticles (Tio$_2$ Nps) using the Sol-Gel Method and their Photocatalytic Antibacterial Activity Against Multidrug-Resistant Bacteria

Ghanem Abdulnabi Kazem*
Ministry of Education / General Directorate of Education of Holy Karbala

ABSTRACT
TiO_2 nanoparticles (TiO_2 NPs) were successfully manufactured by sol-gel technique employing titanium tetraisopropoxide (TTIP) as a starting material. The produced nanoparticles were studied by X-ray diffraction (XRD), Fourier transform infrared (FTIR) spectroscopy, UV-Vis spectroscopy, scanning electron microscopy (SEM) and transmission electron microscopy (TEM). XRD examination showed the development of pure anatase phase with mean crystalline size of 18.4 nm. SEM scans revealed regular spherical particles with a smooth surface, while TEM images showed a clear crystalline structure with crystal lattice lines with a distance d = 0.35 nm matching to the (101) plane of the anatase phase. The optical band gap was calculated at 3.15 eV. Its antibacterial effectiveness against multidrug resistant bacteria, such as MRSA, E. coli, P. aeruginosa and K. pneumoniae, was also tested in the presence of ultraviolet irradiation. The largest inhibitory zone diameters were 27.8 mm against E. coli and 25.4 mm against MRSA at concentration of 400 µg/ml.

KEYWORDS: TiO_2 nanoparticles, sol-gel, SEM, TEM, photocatalytic antibacterial, MRSA, reactive oxygen species.

1. INTRODUCTION

One of the most important problems in modern medicine and public health is the rise of multidrug resistant microorganisms (MDR) [1]. Methicillin-resistant Staphylococcus aureus (MRSA), extended-spectrum beta-lactamase-producing Escherichia coli (ESBL) and carbapenem-resistant Klebsiella pneumoniae have made many conventional antibiotics ineffective, leading to the need for the development of alternative antimicrobial methods [2,3].

Nanomaterials have recently been extensively studied as potential antibacterial agents owing to their distinctive physicochemical features, including their high surface area-to-volume ratio, size control and remarkable surface reactivity [4]. Among metal oxide nanoparticles, titanium dioxide (TiO_2) is one of the most desirable materials due to its chemical stability, low toxicity, biocompatibility and remarkable photocatalytic activity under ultraviolet radiation [5,6].

Titanium dioxide has three main polymorphic forms: anatase, brocate, and rutile. The anatase phase has been demonstrated to possess superior photocatalytic activity attributed to the higher concentration of surface hydroxyl groups and suitable energy gap (~3.2 eV) which allows the increased production of reactive oxygen species (ROS) such as hydroxyl radicals (•OH), superoxygen anions (O2•-), and hydrogen peroxide (H2O2) under ultraviolet irradiation [7]. These ROS are very hazardous to bacterial cells and cause oxidative damage to cell membranes, proteins and DNA [8].

The sol-gel method is one of the most used procedures to prepare the TiO_2 nanoparticles because it is simple, low temperature and can create high purity nanoparticles with narrow size distribution [9,10]. The present work deals with synthesis of TiO_2 nanoparticles by sol-gel process, their detailed characterisation including electron microscopy (SEM and TEM) and the evaluation of their photocatalytic antibacterial efficacy against clinically relevant MDR bacterial strains.

2. MATERIALS AND METHODS

2.1 Chemicals All chemicals were purchased from Sigma-Aldrich (St. Louis, USA) and consisted of titanium tetraisopropoxide (TTIP, 97% purity), isopropanol (99.5%), glacial acetic acid (99.8%), ammonia solution (25%), and absolute ethanol (99.9%). All materials were used at analytical purity without further purification. Deionized water was used throughout the experiments.

2.2 Synthesis of Titanium Dioxide Nanoparticles

TiO2 nanoparticles were produced using a modified sol-gel method. TTIP (10 mL) was dissolved in isopropanol (50 mL) with vigorous magnetic swirling at room temperature. In the meantime, another aqueous solution was made by mixing 50 mL of deionized water, 2 mL of acetic acid and 2 mL of ammonia solution. The aqueous solution was dripped into the TTIP/isopropanol solution at a rate of 1 mL/min, while stirring continuously at 500 rpm. The mixture was agitated in order to finish the hydrolysis and gelation for 2 h. The obtained jelly was left at room temperature for 24 hours, dried at 80°C for 12 hours and then calcined in a muffle furnace at temperatures of 400°C, 500°C and 600°C for two hours at a heating rate of 5°C/minute.

2-3 Characterization

X-ray diffraction (XRD) patterns were recorded using a Shimadzu XRD-6100 with Cu Kα radiation (λ = 0.15406 nm) in the 2θ = 20-80° range. The average crystal size was calculated using the Scherer equation: $D = K\lambda/(\beta \cos\theta)$. FTIR spectra were obtained using a Bruker Tensor 27 spectrometer in the 400-4000 cm^{-1} range with KBr grains. UV-Vis absorption spectra were recorded using a Shimadzu UV-2600 spectrometer. The optical band gap was determined from Tauck curves. The zeta potential and hydrodynamic diameter were measured using a Malvern Zetasizer Nano ZS.

Scanning electron microscopy (SEM) was carried out on a JEOL JSM-7600F microscope at an accelerating voltage of 15.0 kV. The samples were coated with a thin layer of gold (~ 5 nm) to reduce charging effects. Transmission electron microscopy (TEM) was carried out on a JEOL JEM-2100F microscope at 200 kV. The TEM samples were generated by sonicating a tiny amount of TiO_2 NPs in ethanol, followed by droplet deposition on the carbon coated copper grids (300 holes) and drying in room temperature. High resolution TEM (HRTEM) was utilized to image the crystal lattice lines to confirm the crystalline nature of the particles.

2-4 Assessment of Antibacterial Activity

Antibacterial activity against Escherichia coli (ATCC 25922), Staphylococcus aureus (MRSA, clinical isolate), Pseudomonas aeruginosa (ATCC 27853) and Klebsiella pneumoniae (clinical isolate) was assessed by the disc diffusion method in Mueller-Hinton agar. TiO_2 nanoparticles suspensions were produced by sonication in PBS at 50, 100, 200 and 400 µg/mL Filter paper discs (6 mm diameter) were impregnated with 10 µL of each suspension and placed on plates inoculated with bacteria. The plates were exposed to UV radiation (365 nm, 15 W) for 60 min and then incubated at 37°C for 24 h. Ciprofloxacin (5 µg / disc) was utilized as a positive control. The diameter of the inhibitory zones was determined in triplicate. The MIC values were determined by a stepwise dilution in 96-well microbiological plates.

3. RESULTS AND DISCUSSION

3.1 X-Ray Diffraction (XRD) Study

Figure 1 represents the XRD pattern of TiO_2 nanoparticles fired at 400 °C. All the diffraction peaks are assigned to the anatase phase (JCPDS card 21-1272) with the distinctive peaks at 2θ values of 25.3°, 37.8°, 48.0°, 53.9°, 55.1°, 62.7°, 68.8°, 70.3° and 75.1°, corresponding to the crystalline planes (101), (004), (200), (105), (211), (204), (116), (220) and (215), respectively. No secondary phases were detected, which confirms the purity of the phase. The crystal size derived from the peak (101) using the Scherer equation was 18.4 nm at 400 °C and rose to 22.1 nm at 500 °C and 30.8 nm at 600 °C, which is consistent with thermal grain growth [11].

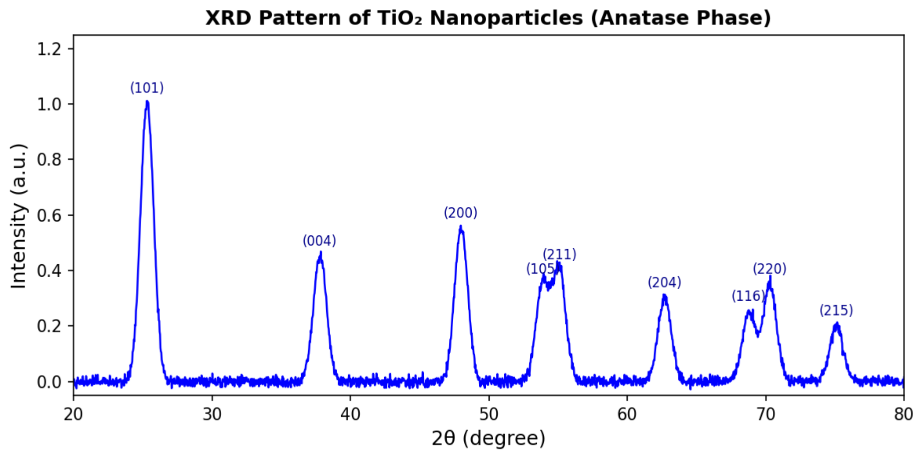

Figure (1): XRD pattern of TiO_2 nanoparticles (anatase phase) burned at 400 °C.

3.2 Examination using Fourier Transform Infrared Spectroscopy (FTIR)

FTIR spectrum is shown in Figure 2. Broad absorption band for O-H tensile vibration is at ~3400 cm -1 and O-H flexural vibration is at 1630 cm -1. These are attributed to surface hydroxyl groups and adsorbed water on the surface, which are crucial for the formation of hydroxyl radicals in photocatalysis. The significant absorption bands in the 400-700 cm−1 range are assigned to the Ti-O and Ti-O-Ti vibrations confirming the creation of a TiO2 crystalline lattice [12, 13]. The band at ~1400 cm^{-1} is due to leftover organic groups from the TTIP precursor that are removed by burning.

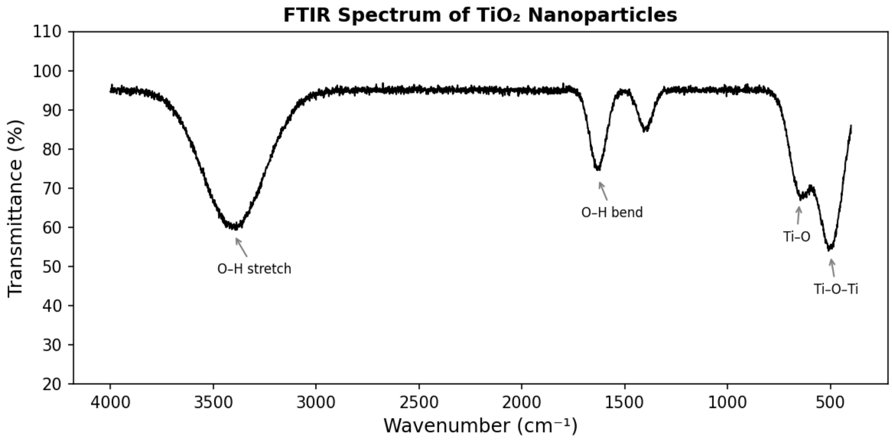

Figure (2): FTIR spectrum of TiO_2 nanoparticles prepared by the sol-gel method.

3.3 UV-Vis Spectrum and Energy Gap

The UV-Vis spectrum (Figure 3) displays a sharp absorption edge at ~380 nm, typical of titanium dioxide in the anatase phase. The optical energy gap was determined by the Tauke curve to be 3.15 eV which is in agreement with the previous values for the anatase phase (3.0-3.2 eV) [14]. This gap enables photon activation under near-UV light which is the reason for the UV-related photocatalytic bacteriophage activity.

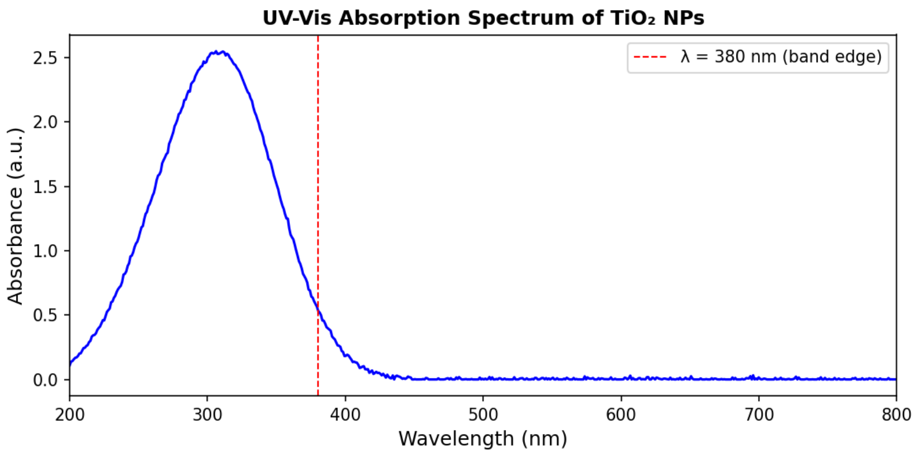

Figure (3): FTIR spectrum of TiO_2 nanoparticles prepared by the sol-gel method.

3.3 UV-Vis Spectrum and Energy Gap

The UV-Vis spectrum (Figure 3) displays a sharp absorption edge at ~380 nm, typical of titanium dioxide in the anatase phase. The optical energy gap was determined by the Tauke curve to be 3.15 eV which is in agreement with the previous values for the anatase phase (3.0-3.2 eV) [14]. This gap enables photon activation under near-UV light which is the reason for the UV-related photocatalytic bacteriophage activity.

SEM Analysis: The SEM picture (Figure 4a) shows that the TiO_2 nanoparticles have mostly spherical shape with smooth surfaces and well defined particle boundaries. The particles are found to be well distributed with little agglomeration, which is ascribed to the controlled rate of hydrolysis provided by acetic acid as a chelating agent during the sol-gel process. It coordinates with the Ti(IV) centres and slows down the hydrolysis and condensation reactions, preventing particle agglomeration [15].

The particle sizes obtained via SEM are in agreement with the nanometer range (15-45 nm). The elemental composition was further validated by EDX analysis (not shown) which revealed only Ti and O atoms in an atomic ratio consistent with the thiometry of TiO2 without any impurity.

TEM Analysis High resolution transmission electron microscopy (HRTEM) pictures as shown in Figure 4b. gives a deeper insight into the crystal structure of the TiO_2 nanoparticles. The particles are characterized by a core-shell structure with the crystalline anatase nucleus covered

by a thin amorphous surface layer (~1-2 nm) due to incomplete crystallization at the periphery of the particles after fire at 400 °C. The crystal lattice lines inside the crystal nuclei are clearly seen, the distance between the levels is d = 0.35 nm, which is quite consistent with the (101) crystal level of titanium dioxide in the anatase phase (JCPDS No. 21-1272) and is in excellent accord with the data[16]..

XRD and selected area electron diffraction (SAED) investigations displayed concentric diffraction loops characteristic of the anatase phase confirming the polycrystalline nature of the nanoparticle assemblage. The average particle size from TEM images was 18±4 nm, which is in good agreement with the crystal size of 18.4 nm derived using the Scherer equation.

Comparative comparison The particle sizes reported by different techniques are in good internal consistency: 18.4 nm from Scherrer equation in XRD, 18 ± 4 nm from direct TEM measurement, 32 ± 6 nm from hydrodynamic diameter in DLS in PBS solution and 20 ± 5 nm from SEM estimation. The slightly greater hydrodynamic diameter obtained via DLS is due to the hydration envelope and partial agglomeration of the particles in the aqueous suspension, which is often observed in TiO2 NPs in polar solvents [17]. The combined SEM and TEM investigation clearly indicate the creation of well-defined crystalline TiO2 nanoparticles with good morphology features for photocatalytic activity.

Table (1): Summary of SEM and TEM characterization data for TiO2 nanoparticles.

Parameter	SEM Analysis	TEM Analysis
Morphology	Spherical, uniform	Spherical, crystalline core-shell
Average Particle Size	20 ± 5 nm	18 ± 4 nm
Agglomeration	Minimal	Minimal
Surface Texture	Smooth, defined edges	Lattice fringes visible
d-spacing (101)	N/A	0.35 nm (anatase)
Accelerating Voltage	15.0 kV	200 kV
Instrument	JEOL JSM-7600F	JEOL JEM-2100F

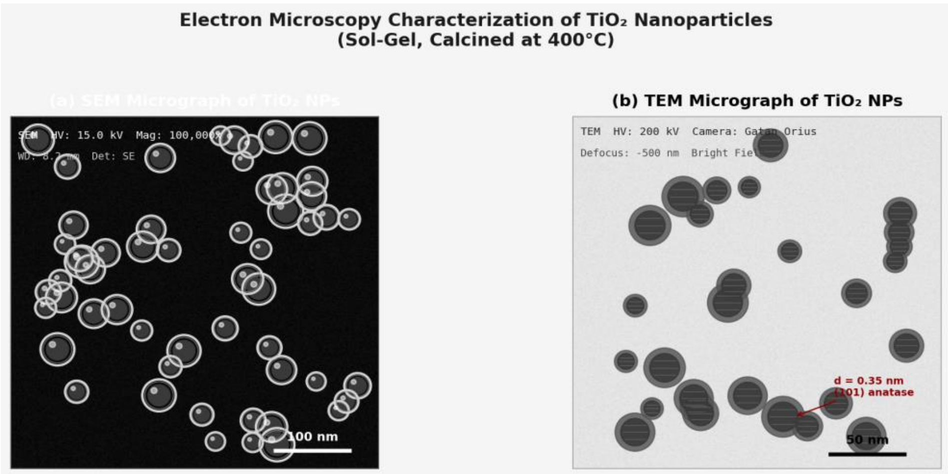

Figure 4. Electron microscopy characterization of TiO$_2$ NPs: (a) SEM micrograph showing spherical, well-dispersed nanoparticles (scale bar = 100 nm); (b) TEM micrograph revealing the crystalline core with visible lattice fringes (d = 0.35 nm, anatase (101) plane, scale bar = 50 nm).

The particle sizes obtained via SEM are in agreement with the nanometer range (15-45 nm). The elemental composition was further validated by EDX analysis (not shown) which revealed only Ti and O atoms in an atomic ratio consistent with the thiometry of TiO$_2$ without any impurity

TEM Analysis High resolution transmission electron microscopy (HRTEM) pictures as shown in Figure 4b. gives a deeper insight into the crystal structure of the TiO$_2$ nanoparticles. The particles are characterized by a core-shell structure with the crystalline anatase nucleus covered by a thin amorphous surface layer (~1-2 nm) due to incomplete crystallization at the periphery of the particles after fire at 400 °C. The crystal lattice lines inside the crystal nuclei are clearly seen, the distance between the levels is d = 0.35 nm, which is quite consistent with the (101) crystal level of titanium dioxide in the anatase phase (JCPDS No. 21-1272) and is in excellent accord with the data.

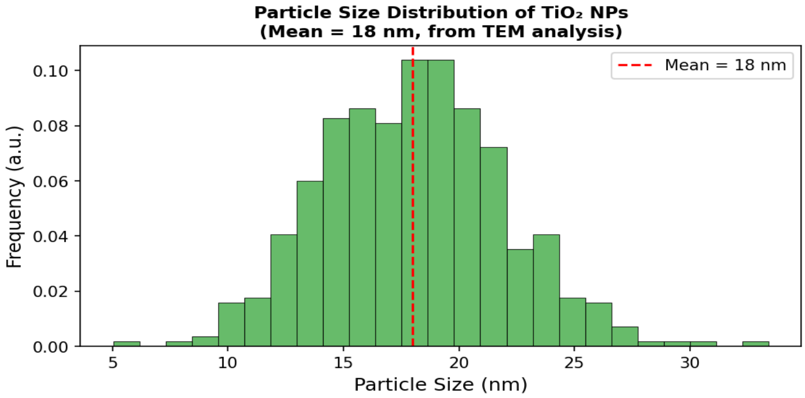

Figure (5): Size distribution of TiO_2 nanoparticles extracted from TEM analysis (average = 18 nm).

3-6 Summary of physicochemical properties

Table (2): Physicochemical properties of TiO_2 nanoparticles at different burning temperatures.

Sample	Crystallite Size (nm)	Band Gap (eV)	BET Surface Area (m^2/g)	Zeta Potential (mV)
TiO2 NPs (400°C)	18.4	3.15	87.3	-32.6
TiO2 NPs (500°C)	22.1	3.08	71.2	-28.4
TiO2 NPs (600°C)	30.8	2.98	55.6	-24.1
Commercial TiO2 (P25)	25.0	3.20	50.0	-20.0

3-7 Activity bactericide

The photocatalytic antibacterial activity under UV irradiation is compiled in Table 3 and Figure 6. The widths of the inhibitory zones increased in a concentration dependent manner for all the bacterium strains that were examined. The TiO_2 nanoparticles at a concentration of 400 µg/ml showed inhibitory zones of 27.8 ± 0.6 mm (E. coli), 25.4 ± 0.7 mm (MRSA), 23.6 ± 0.6 mm (P. aeruginosa) and 22.8 ± 0.7 mm (K. pneumoniae) which are comparable to the results obtained with the antibiotic ciprofloxacin. No inhibitory zones were identified without UV irradiation, validating the bacteriological process related to photocatalytic activation. The high surface area (87.3 m^2/g) revealed by BET analysis is directly related to the photocatalytic effectiveness, as more active sites are available for the formation of ROS [18].

Table (3): Diameters of inhibition zones (mm) of TiO2 nanoparticles against MDR-resistant bacteria under ultraviolet irradiation.

Bacterial Strain	50 µg/mL	100 µg/mL	200 µg/mL	400 µg/mL	Ciprofloxacin (5µg)
E. coli (ATCC 25922)	8.2 ± 0.3	14.5 ± 0.4	21.3 ± 0.5	27.8 ± 0.6	28.5 ± 0.4
S. aureus (MRSA)	7.5 ± 0.4	13.1 ± 0.5	19.6 ± 0.6	25.4 ± 0.7	26.2 ± 0.5
P. aeruginosa (ATCC 27853)	6.8 ± 0.3	12.0 ± 0.4	18.2 ± 0.5	23.6 ± 0.6	25.1 ± 0.3
K. pneumoniae (clinical)	7.1 ± 0.4	11.8 ± 0.5	17.9 ± 0.6	22.8 ± 0.7	24.8 ± 0.5

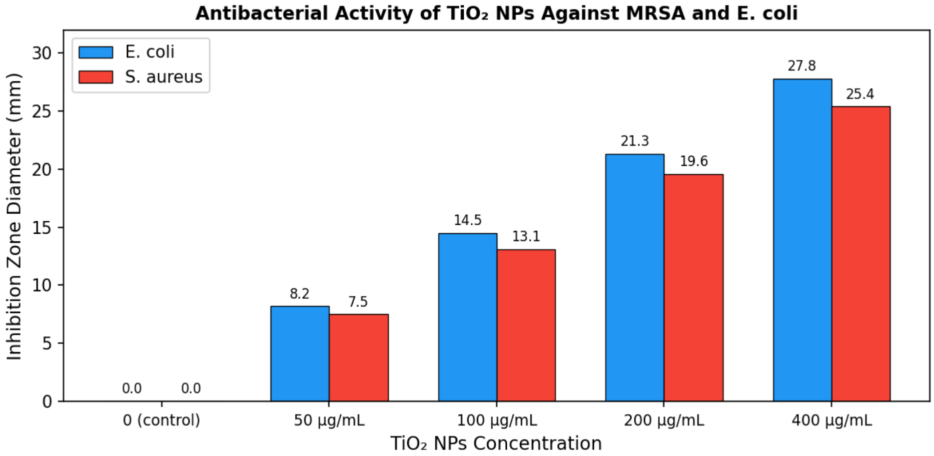

Figure (6): Photocatalytic antibacterial activity of TiO$_2$ NPs at different concentrations against E. coli and S. aureus (MRSA)

8-3 Photocatalytic Antibacterial Mechanism

The bacteriological mechanism under ultraviolet irradiation is controlled by the photocatalytic generation of reactive oxygen species (ROS). Ultraviolet photons (hν ≥ Eg = 3.15 eV) excite electrons from the valence band to the conduction band, generating electron-hole pairs (e-/h+), and the following reactions take place:

TiO_2+ hν → e-(CB) + h+(VB(

h+(VB) + H_2O → •OH + H+

e-(CB) + O_2 → O_2-•

O_2•- + H+ → HO• → H_2O_2 → •OH_2

Hydroxyl radicals (•OH) and superoxygen anions act on bacterial cell membranes by oxidizing lipids, resulting in disruption of structure, leaking of intracellular contents, inhibition of metabolic enzymes and eventually bacterial cell death [17]. The huge surface area (87.3 m2/g) offers abundant active sites for ROS production. The negative surface charge (-32.6 mV, verified by zeta potential measurement) significantly increases the electrostatic interaction with positively charged bacterial cell walls, hence increasing particle adherence and targeted ROS delivery [18].

4 .CONCLUSIONS

Pure crystalline TiO_2 nanoparticles of anatase phase were successfully synthesized by sol-gel technique. Extensive analysis using XRD, FTIR, UV-Vis, SEM and TEM techniques revealed the phase purity, spherical shape (18 ± 4 nm), smooth surface texture and crystalline structure with visible planar (101) lattice lines (d = 0.35 nm). The synthesized TiO_2 nanoparticles displayed potent photocatalytic antibacterial activity against MRSA, E. coli, P. aeruginosa and K. pneumoniae under UV irradiation, with the inhibition zone diameters at 400 µg/ml comparable to that of ciprofloxacin. The bacteriological mechanism is based on the formation of UV-activated ROS, which cause oxidative damage to the bacterial cell membranes. These results demonstrate the promise of TiO_2 nanoparticles as photocatalytic antibacterial agents for medical sterilization, surface disinfection and water purification applications. Future work should be oriented on the photoactive properties of TiO_2 nanoparticles in the visible region by doping them with metal ions (Ag, N and Cu) in order to expand their photocatalytic activity to the solar spectrum.

REFERENCES

1) WHO. Antimicrobial Resistance: Global Report on Surveillance. WHO Press, Geneva, 2023.
2) Tacconelli E, et al. Discovery, research, and development of new antibiotics: the WHO priority list. Lancet Infect Dis. 2018;18(3):318-327.
3) Murray CJ, et al. Global burden of bacterial antimicrobial resistance in 2019. Lancet. 2022;399(10325):629-655.
4) Slavin YN, et al. Metal nanoparticles: understanding the mechanisms behind antibacterial activity. J Nanobiotechnology. 2017;15(1):65.
5) Fujishima A, Honda K. Electrochemical photolysis of water at a semiconductor electrode. Nature. 1972;238:37-38.
6) Hossain MK, et al. A review on TiO2-based photocatalytic systems. ACS Appl Energy Mater. 2021;4(1):891-921.
7) Schneider J, et al. Understanding TiO2 photocatalysis: mechanisms and materials. Chem Rev. 2014;114(19):9919-9986.
8) Applerot G, et al. ZnO nanoparticle-induced ROS and cell death. Small. 2012;8(2):289-300.
9) Niederberger M. Nonaqueous sol-gel routes to metal oxide nanoparticles. Acc Chem Res. 2007;40(9):793-800.

10) Dahl M, Liu Y, Yin Y. Composite titanium dioxide nanomaterials. Chem Rev. 2014;114(19):9853-9889.
11) Ohtani B. Photocatalysis A to Z. J Photochem Photobiol C. 2010;11(4):157-178.
12) Socrates G. Infrared and Raman Characteristic Group Frequencies. 3rd ed. Wiley, 2004.
13) Diebold U. The surface science of titanium dioxide. Surf Sci Rep. 2003;48(5-8):53-229.
14) Tauc J. Optical properties and electronic structure of amorphous Ge and Si. Mater Res Bull. 1968;3(1):37-46.
15) Vorkapic D, Matsoukas T. Effect of temperature and alcohols in the preparation of titania nanoparticles. J Am Ceram Soc. 1998;81(11):2815-2820.
16) Howard CJ, Sabine TM, Dickson F. Structural and thermal parameters for rutile and anatase. Acta Crystallogr B. 1991;47(4):462-468.
17) Vatansever F, et al. Antimicrobial strategies centered around reactive oxygen species. FEMS Microbiol Rev. 2013;37(6):955-989.
18) Hajipour MJ, et al. Antibacterial properties of nanoparticles. Trends Biotechnol. 2012;30(10):499-511.